IEEE Access
Multidisciplinary | Rapid Review | Open Access Journal

Received November 20, 2018, accepted December 20, 2018, date of publication December 28, 2018,
date of current version January 23, 2019.

Digital Object Identifier 10.1109/ACCESS.2018.2889929

A Precise and Stable Segmentation Algorithm of SAR Images Based on Random Weighting Method and Modified Level Set

SHANSHAN LIN[1,2], XIANBIN WEN[1,2], HAIXIA XU[1,2], LIMING YUAN[1,2], AND QINGXIA MENG[3]

[1]Key Laboratory of Computer Vision and System, Ministry of Education, Tianjin University of Technology, Tianjin 300384, China
[2]Tianjin Key Laboratory of Intelligence Computing and Novel Software Technology, Tianjin University of Technology, Tianjin 300384, China
[3]School of Computer Science and Technology, Tianjin University, Tianjin 300350, China

Corresponding author: Xianbin Wen (xbwen317@163.com)

This work was supported in part by the National Natural Science Foundation of China under Grant 61472278, in part by the Key Project of Natural Science Foundation of Tianjin University under Grant 2017ZD13, and in part by the Research Project of Tianjin Municipal Education Commission under Grant 2017KJ255.

ABSTRACT Level set methods have been widely used for image segmentation due to their good boundary detection accuracy. In the context of synthetic aperture radar (SAR) image segmentation, the presence of speckles and the distribution estimation of SAR image remain important issues that may hinder the accuracy of any segmentation method based on level set methods. In this paper, we propose a more accurate and a stable segmentation method based on the random weighting method and modified threshold-based level set energy functional. The proposed method uses a level set evolution that is based on the minimization of an objective energy functional, whose propagation function is based on the $\mathcal{G}^0$ statistical model, whose parameters are estimated by random weighting estimators, and the estimator is not affected by the hypothesized model and sampling number. In addition, a new regularization item and length term, which maintain the regularity of the level set function and contour respectively, were employed. The experimental results demonstrate that the proposed methodology has a good and stable capability of segmentation, both in homogeneous, heterogeneous, and extremely heterogeneous regions in SAR image.

INDEX TERMS Level set, random weighting estimators (RWE), segmentation, synthetic aperture radar.

I. INTRODUCTION

Synthetic Aperture Radar (SAR), which allows day-and-night and all-weather acquisitions, is an advanced active microwave device for earth observation. Therefore, it plays an utterly significant role in the national economy and military applications [1]. Segmentation plays an important role in the automatic analysis and interpretation of SAR images. However, the inherent multiplicative noise, known as speckle, which originates from the interference of the coherent wavefronts, is specific to active imaging systems and considerably degrades the registered imagery [2]. As a consequence, standard segmentation methods that have been validated for optical data do not report satisfying results when applied directly to SAR images. Another difficulty is the heterogeneity of urban areas in SAR images that leads to heterogeneous statistical modeling, reflecting different ground materials such as asphalt, concrete, and metal.

In recent years, much work has been done on the segmentation of SAR images, such as the edge detection [3], clustering methods [4], superpixel-based methods [5], and model-based methods [6]. However, each method has both advantages and disadvantages. Among various segmentation methods, the level set method, which has emerged in the last three decades, has unmatched performance in computer vision [7]. They offer novel ways to segment SAR images. Liu *et al.* proposed a SAR image segmentation method based on a reaction diffusion (RD) level set evolution equation in an active contour model [8]. Zhang et al. gave an energy functional based on an edge-region active contour model for SAR image segmentation [9]. Compared to other methods, the level set method has advantages such as easy integration of image features, robustness to noise, and natural representation of boundaries and regions. Nevertheless, even such methods have some limitations, namely, low segmentation accuracy

and unstable segmentation results. In addition, the statistical property of SAR images is often utilized to ensure the robustness of derived models to the speckle noise in those methods [8]. Research studies have proved that the precise statistical model could significantly improve the segmentation accuracy of statistical model-based level sets [10]. Various distribution models, such as the K [11], gamma [12], Weibull [13] and $\mathcal{G}$ distributions [14], have been used to model the statistical property of SAR images. For the K and Gamma distribution, modeling extremely heterogeneous regions is unsatisfactory. The Weibull distribution is not suitable for multi-look SAR data and its parameters estimation has a tremendous challenge. Compared to other distributions, the $\mathcal{G}^0$ distribution has outstanding performance in modeling SAR images with homogeneous, heterogeneous and extremely heterogeneous regions [15].

The $\mathcal{G}^0$ distribution is characterized by the number of looks L, scale parameter α, and roughness parameter γ. Accurate parameters are essential to describe different regions in a SAR image. Obviously, the accuracy in the parameter estimation becomes very important. Several parameter estimation methods have been proposed, such as the method of moments (MOM) [16], [17], maximum likelihood estimation (MLE) [11], method of log-moment estimation (MOLC) [18]. All these estimation methods are based on the large sample theory. In fact, processing and interpreting SAR images is a small-sample problem. For instance, image filtering requires few observations within a window. Its parameter estimation with small samples is subject to many problems, in particular bias, large variance, and sensitivity to deviations from the hypothesized model. In contrast, the $\mathcal{G}^0$ distribution is a heavy-tailed distribution. Therefore, dealing with SAR data is inherently difficult because samples from the tail of the distribution will have a strong influence on parameter estimation. Wang [19] proposed techniques to address this issue, although at the cost of additional computational load.

The random weighting method, introduced by Zheng [20], is an intriguing nonparametric method for computing the standard error, the bias or confidence intervals, and for testing the null hypothesis with limited data [21]. One of the advantages of this method is that it is better than the Bootstrap method in small-sample cases. Wang et al. applied RWE to the $\mathcal{G}^0$ distribution, and verified that RWE can estimate better parameter values with small samples in a 3×3 sliding window [19].

In this paper, to resolve the above problems, we focus on the segmentation of SAR images based on $\mathcal{G}_I^0$ distribution modeling, Random Weighting Estimator, and improved level-set methods. We utilize the $\mathcal{G}_I^0$ distribution for intensity SAR image modeling, and Random Weighting Estimators (RWE) for parameters estimation. Then, Entropy Processing (EP) is used for roughness and scale parameter to improve SAR image segmentation performance based on the improved threshold-based level set (ITLS).

The remainder of the article is organized as follows. In the next section, we introduce methods for SAR image segmentation. Firstly, we review the $\mathcal{G}^0$ model for speckled SAR data and its parameter estimation methods with an emphasis on the random weighting method. In addition, EP of parameters, and ITLS are also introduced in this section. Methodology analysis, experiment results and the stability analysis of ITLS are given in section 3. Section 4 draws the conclusions and summarizes the article.

II. STATISTICAL DISTRIBUTION AND PARAMETER ESTIMATION

A. STATISTICAL MODEL FOR SAR DATA

Numerous statistical models are proposed for describing property of SAR images, for instance, Rayleigh and exponential distribution for single-look SAR images, Gamma distribution for multi-look SAR images, K distribution following multiplicative model. However, these statistical models are not suitable for highly heterogeneous areas. The $\mathcal{G}^0$ model used in [16]–[18] and [22] can address this issue.

X and Y are two independent and unobserved random fields. Random field X follows an inverse-gamma distribution that models the terrain backscatter and Y follows a gamma distribution that models the speckle noise. Then, the $\mathcal{G}^0$ distribution follows the multiplicative law $Z = X \times Y$ [23]. In this paper, the probability density functions (PDF) for amplitude SAR images and intensity SAR images can be written as follows:

$$f_{\mathcal{G}_A^0}(z,\alpha,\gamma,L) = \frac{2L^L\Gamma(L-\alpha)}{\gamma^\alpha\Gamma(-\alpha)\Gamma(L)}\frac{z^{2L-1}}{(\gamma+z^2L)^{L-\alpha}}, \quad -\alpha,\gamma,z>0, \quad L\geq 1 \tag{1}$$

$$f_{\mathcal{G}_I^0}(z,\alpha,\gamma,L) = \frac{L^L\Gamma(L-\alpha)}{\gamma^\alpha\Gamma(-\alpha)\Gamma(L)}\frac{z^{L-1}}{(\gamma+zL)^{L-\alpha}}, \quad -\alpha,\gamma,z>0, \quad L\geq 1 \tag{2}$$

which are denoted by $\mathcal{G}_A^0(\alpha,\gamma,L)$ and $\mathcal{G}_I^0(\alpha,\gamma,L)$, respectively. The r-order moments are given by

$$E_{\mathcal{G}_A^0}(Z^r) = \left(\frac{\gamma}{L}\right)^{r/2}\frac{\Gamma(-\alpha-r/2)\Gamma(L+r/2)}{\Gamma(-\alpha)\Gamma(L)} \tag{3}$$

$$E_{\mathcal{G}_I^0}(Z^r) = \left(\frac{\gamma}{L}\right)^{r}\frac{\Gamma(-\alpha-r)\Gamma(L+r)}{\Gamma(-\alpha)\Gamma(L)} \tag{4}$$

For all these formulae, α characterizes the roughness of the SAR data and γ characterizes the scale of the SAR data, and L is the number of looks. In this paper, L is assumed to be known and constant for all pixels of SAR images. Fig. 1 shows the pdf of the $\mathcal{G}_I^0$ distribution with different parameters.

B. RANDOM WEIGHTING ESTIMATOR

The method of moments was introduced by British statistician K. Pearson at the end of the 19th century and its theory is based on the law of large numbers. The idea behind this estimation method is to make the r-order moments of samples equal to the r-order moments of population. The method of moments has successfully been employed to estimate the parameters of the $\mathcal{G}_A^0$ distribution [16], [17], [24], [25]. Let $Z_1,\ldots,Z_n$ be independent and identically distributed random

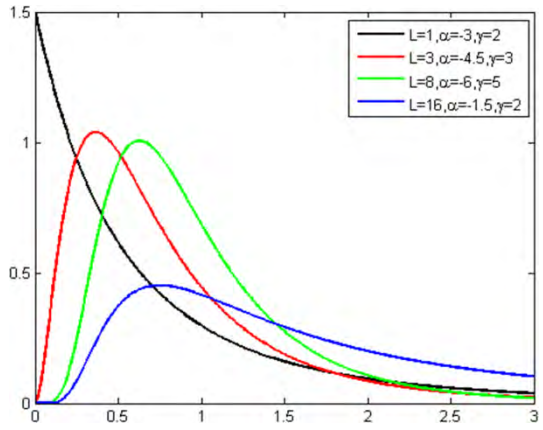

FIGURE 1. Effect of parameters (number of looks L, roughness α, and scale γ) on the $\mathcal{G}_I^0$ distribution.

variables with $Z \sim \mathcal{G}_I^0(\alpha, \gamma, L)$, $\alpha < -1/2$, $\gamma > 0$ and L known. Then, the r-th sample moment is given as follows:

$$\bar{Z}_n^r = \frac{1}{n}\sum_{i=1}^{n} Z_i^r \tag{5}$$

The random weighting estimation of the $\bar{Z}_n$ and $\bar{Z}_n^r$ can be defined as

$$H_n = \sum_{i=1}^{n} V_i X_i \tag{6}$$

and

$$H_n^r = \sum_{i=1}^{n} V_i X_i^r \tag{7}$$

where $(V_1, V_2, \ldots, V_n)$ is a random vector subject to Dirichlet distribution $D(1, 1, \ldots, 1)$, that is, $\sum_{i=1}^{n} V_i = 1$ and the joint density function of $(V_1, V_2, \ldots, V_n)$ is

$$f(V_1, V_2, \ldots, V_n) = \Gamma(n) \tag{8}$$

where $(V_1, V_2, \ldots, V_n) \in D_n$ and $D_{n-1} = \{(V_1, V_2, \ldots, V_{n-1}) : V_i \geq 0, (i = 1, 2, \ldots, n-1), \sum_{i=1}^{n-1} V_i \leq 1\}$.

Replacing the population moments by their sample counterparts, and the parameters by the corresponding estimators, in Eq. (4) and Eq. (5), yields to the following system of equations

$$\bar{Z}_n = \left(\frac{\hat{\gamma}}{L}\right) \frac{\Gamma\left(-\hat{\alpha}-1\right)\Gamma\left(L+1\right)}{\Gamma\left(-\hat{\alpha}\right)\Gamma\left(L\right)}, \quad -\hat{\alpha} > 1 \tag{9}$$

$$\bar{Z}_n^{\frac{1}{2}} = \left(\frac{\hat{\gamma}}{L}\right)^{\frac{1}{2}} \frac{\Gamma\left(-\hat{\alpha}-(1/2)\right)\Gamma\left(L+(1/2)\right)}{\Gamma\left(-\hat{\alpha}\right)\Gamma\left(L\right)}, \quad -\hat{\alpha} > 1/2 \tag{10}$$

This leads to the following equation that can be solved numerically in order to obtain the moment estimator for α

$$\frac{\bar{Z}_n \Gamma\left(-\hat{\alpha}\right)\Gamma\left(L\right)L}{\Gamma\left(-\hat{\alpha}-1\right)\Gamma\left(L+1\right)} = \frac{(\bar{Z}_n^{\frac{1}{2}})^2 \Gamma^2\left(-\hat{\alpha}\right)\Gamma^2\left(L\right)L}{\Gamma^2\left(-\hat{\alpha}-1/2\right)\Gamma^2\left(L+(1/2)\right)} \tag{11}$$

$\bar{Z}_n$ and $\bar{Z}_n^{1/2}$ are replaced by their random weighting estimation H_n, $H_n^{1/2}$ in (11), respectively. We have

$$\frac{H_n \Gamma\left(-\hat{\alpha}\right)\Gamma\left(L\right)L}{\Gamma\left(-\hat{\alpha}-1\right)\Gamma\left(L+1\right)} = \frac{(H_n^{\frac{1}{2}})^2 \Gamma^2\left(-\hat{\alpha}\right)\Gamma^2\left(L\right)L}{\Gamma^2\left(-\hat{\alpha}-1/2\right)\Gamma^2\left(L+(1/2)\right)} \tag{12}$$

Therefore, the random weighting estimator $\hat{\alpha}$ for α can be obtained via solving Eq. (12). By plugging the value of $\hat{\alpha}$ into Eq. (13), we obtain random weighting estimator $\widehat{\gamma}$

$$\widehat{\gamma} = \overline{Z}_n(-\widehat{\alpha} - 1) \tag{13}$$

Practical experiments have been conducted to estimate the α and γ parameters with $\mathcal{G}_I^0$ distribution modeling the real SAR image by random weighting estimator. Fig. 2(a) is an intensity SAR image with three looks, and its yellow rectangular area was used as the sample to estimate parameters. In the sample area, 25 random intensity values (small sample) are selected to estimate the α and γ parameters. Fig. 2(b) displays the histogram and the line of the estimated probability density function by MOM, MLE, MOLC, and RWE for the rectangular region in Fig. 2(a). The Kolmogorov–Smirnov (K-S, one of the criteria for evaluating the accuracy of parametric modeling) test was then performed between X from the image and Y for the null hypothesis H_o"both samples come from the same distribution," and the complementary alternative hypothesis. The sample p value of the K-S test of RWE is 0.7158, which is higher than that of other methods. This improves RWE to have good estimation performance with small samples.

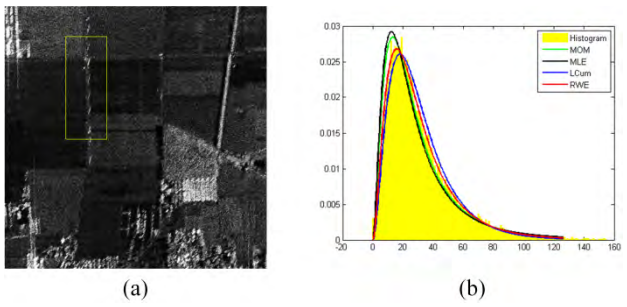

FIGURE 2. Fitting of a SAR image region. (a) is a real SAR image, the yellow region of (b) is the histogram of the yellow rectangular region of (a), and the lines of (b) are the estimated probability density function by MOM, MLE, MOLC, and RWE.

III. SAR IMAGES SEGMENTATION

A. PREPROCESSING

In order to better distinguish different regions of a SAR image, we use Entropy Processing (EP), which deals with the estimators of roughness and scale parameters. According to [17], the formula of Renyi entropy is defined as

$$H_q(P) = \frac{1}{1-q} \ln \int f^q(x) dx \tag{14}$$

where $f(x)$ is probability density function of a distribution. For the $\mathcal{G}_I^0$ distribution, the entropy equation is expressed as

$$H_{\mathrm{q}}(\mathcal{G}_I^0) = \frac{1}{1-q}\ln\int_0^{\infty}\left[\frac{L^L\Gamma(L-\alpha)}{\gamma^{\alpha}\Gamma(-\alpha)\Gamma(L)}\frac{z^{L-1}}{(\gamma+zL)^{L-\alpha}}\right]^q dz \tag{15}$$

where the parameter q is essential to adjust the sensitivity of the entropy to the shape of the probability density function [17]. And we set $q = 4$ according to [17].

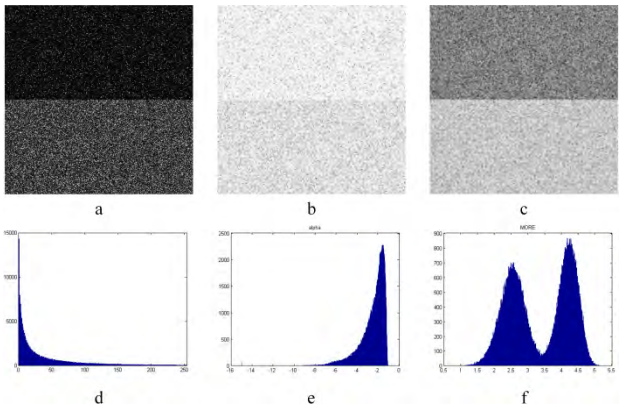

FIGURE 3. (a) is a two-region simulated SAR image (one look) and (d) is its histogram; (b) is the estimated roughness map of (a) and (e) is its histogram; (c) is the EP map of (a) and (f) is its histogram.

In Fig. 3, (a) is a synthetic SAR image with two regions that the upper area follows $\mathcal{G}_I^0(-1.5, 1, 1)$ and another is $\mathcal{G}_I^0(-4.5, 3, 1)$; (d) is the histogram of (a). Fig. 3(b) displays the roughness map of the original synthetic SAR image (a) and (e) is its histogram. Fig. 3(c) is the EP map of (a) and (f) is its histogram. Fig. 3(c) and (f) show the strong capabilities of EP to discriminate different regions of SAR images. Consequently, the segmentation methods based on threshold are adequate for practical applications.

B. THE IMPROVED THRESHOLD-BASED LEVEL SET

In this section, we adopted and improved the method of the threshold-based level set. The level set theory, formulated by Sethian, is based on the Hamilton-Jacobi equation [26]. It states that a closed curve $\vec{\phi}(t) = \{x|\psi(x,t) = 0\}, x \in \mathbb{R}^n$ evolves with a velocity field $(\pm F\vec{\eta})$, where F is the speed function and $(\pm\vec{\eta})$ is the unit vector that is perpendicular to $\vec{\phi}$. In the discrete domain, the evolution equation is

$$\psi^{k+1} = \psi^k + \Delta t(F_{prop} + \varepsilon K)|\nabla\psi^k| \tag{16}$$

where ψ^k is the level set function, Δt is the time step, the operator $|\nabla\psi^k|$ stands for the gradient magnitude, and $\varepsilon \in \mathbb{R}$ [9], [26]. The velocity term comprises of a propagation term F_{prop}(speed function), which minimizes a cost function, and a regularization term based on the curvature K of ψ^k.

In order to achieve better regularization, a new evolution equation for smoother segmentation results was proposed in this section. The proposed evolution equation of level set is given by

$$\psi^{k+1} = \psi^k + \Delta t(F_{prop} + \nu\delta_\sigma(\psi^k)|\nabla\psi^k| + \mu(\nabla^2\psi^k - |\nabla\psi^k|)) \tag{17}$$

In formula (17), to make better use of EP map, F_{prop}, a new propagation function is redefined. In [27], F_{prop} is computed using the intensity matrix of SAR images, i.e., the backscatter of the pixels

$$F_{prop} = \begin{cases} I(x,y) - I_{lower}, & I(x,y) < I_{average} \\ I_{higher} - I(x,y), & I(x,y) \geq I_{average} \end{cases} \tag{18}$$

where $I(x, y)$ is the intensity matrix of the SAR image, and $I_{average}$, the threshold of $I(x, y)$, is computed by $I_{average} = (I_{lower} + I_{higher})/2$. In this paper, the new F_{prop} is:

$$F_{prop} = \begin{cases} EP(x,y) - T_{EP}, & EP(x,y) < T_{EP} \\ T_{EP} - EP(x,y), & EP(x,y) \geq T_{EP} \end{cases} \tag{19}$$

where() $EP(x, y)$ is the value of EP matrix at (x, y), T_{EP} is calculated by the Otsu method utilizing the EP map. The propagation function F_{prop} plays a key role in driving the active contour toward object boundaries.

In addition, the length term $\nu\delta_\sigma(\psi^k)|\nabla\psi^k|$ and the level set regularization term $\mu(\nabla^2\psi^k - |\nabla\psi^k|)$ were added in formula (17). In the length term and regularization term, $|\nabla\psi^k|$ is the curvature of the planar curve ψ^k, μ and ν is the adjustment parameters and $\delta_\sigma(\psi^k)$ is an approximation of the Dirac function, expressed as

$$\delta_\sigma(\psi^k) = \frac{1}{\pi}\cdot\frac{\sigma}{\sigma^2 + (\psi^k)^2} \tag{20}$$

The length term has a length smoothing or shortening effect on the zero-level contour, which is indispensable to maintain the regularity of the contour. The regularization term serves to maintain the regularity of the level set function. The length term and the regularization term are known to have a good smoothing effect in [28].

IV. EXPERIMENTS

In this section, we first introduce the method to evaluate the segmentation performance quantitatively. After that, we discuss the choice of segmentation method and sliding window size by experiments on both simulated and real SAR images. In addition, we performed experiments on both synthetic and real SAR images using the methods in [9] and [17] and the proposed method. Our code was implemented in Matlab R2014a running on a laptop with an Intel i7 at 3.3GHz.

A. METHOD OF PERFORMANCE EVALUATION

To verify the performance of the proposed segmentation methodology based on the random weighting method, both synthetic and real intensity SAR images were used for the experiment. The Mean Square Error (MSE), Error of Segmentation (EOS) and Region Fitting Error (RFE) were used as the evaluation criteria. The MSE were calculated as:

$$MSE = \frac{sum((\widehat{\alpha} - \alpha)^2)}{N_{piexls}} \tag{21}$$

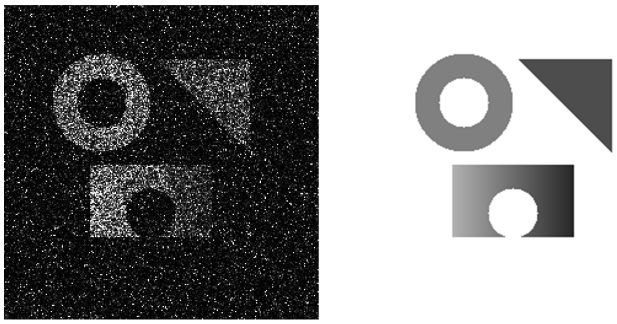

(a) (b)

FIGURE 4. (a) is a synthetic SAR image, which follows the $\mathcal{G}_I^0$ distribution, (b) is the ground truth.

where $\widehat{\alpha}$ is the estimated roughness values of each image pixel, α is the standard value of roughness, and N_{piexls} is the pixel number of the simulated SAR image. Smaller MSE means higher estimation accuracy. EOS is expressed as:

$$EOS = \frac{\#(M)}{\#(IF)} \tag{22}$$

where $\#(M)$ is the number of mis-segmented pixels and $\#(IF)$ is the area of targets. The RFE can be expressed as

$$RFE = \frac{\max(A(\Omega_g), A(\Omega_s)) - A(\Omega_g \cap \Omega_s)}{\max(A(\Omega_g), A(\Omega_s))} \tag{23}$$

where $A(\Omega_g)$ and $A(\Omega_s)$ is the area of the ground truth and the segmented image. Small EOS and RFE mean good segmentation results.

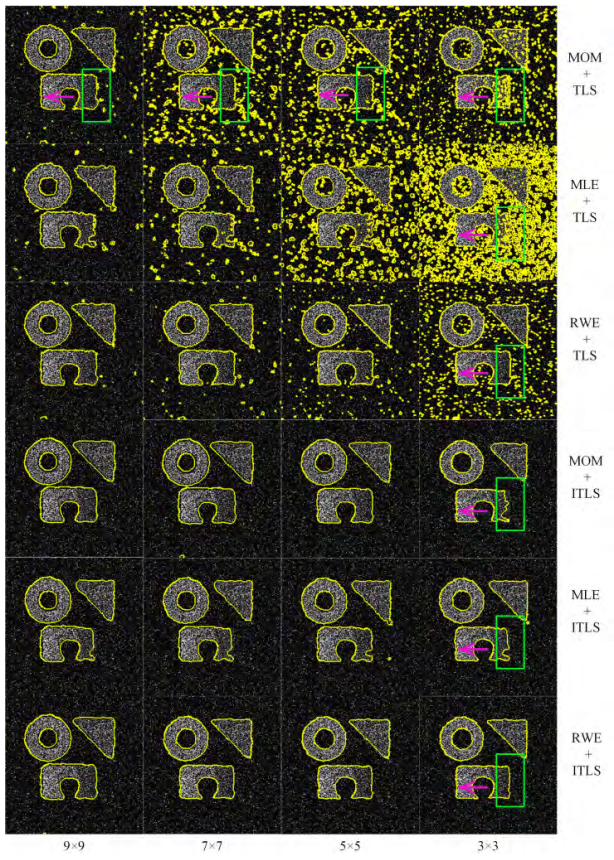

FIGURE 5. Segmentation results of Fig. 4(a) with different methods and different sliding windows. The sliding window size and the segmentation methods are at the bottom and right of the picture respectively.

B. METHOD ANALYSIS

To demonstrate the performance of our algorithm, we did method analysis on both simulated and real SAR images. In the first place, MOM, MLE and RWE are utilized to estimate

the roughness and scale parameters of each pixel of the SAR images. The sizes of the sliding windows for estimation were 9×9, 7×7, 5×5, and 3×3. After that, we combined the different estimation methods with the threshold-based level set (TLS) proposed [17] and the improved threshold-based level set (ITLS) method proposed in this paper to obtain segmentation results.

In Fig. 4, the simulated image (a) is generated from original image (b) by adding multiplicative speckle noise with different $\mathcal{G}_I^0$ distributions to the background and target. The foreground of Fig. 4(a) follows $\mathcal{G}_I^0$ $(-3, 2, 1)$ and its background follows $\mathcal{G}_I^0$ $(-1.5, 1, 1)$. Fig. 5 shows the segmentation results with different level set methods and different parameter estimation methods in different sliding windows. In Fig. 5, the segmentation results of the same column have the same sliding window size and the segmentation results of the same row have the same segmentation methods. The first three rows are the results of MOM, MLE, and RWE with TLS in 9×9, 7×7, 5×5, and 3×3. Although the larger window can suppress the speckle noise to some extent, the contour cannot stop at the accurate objects boundaries. Because the large window can blur boundaries when the window are cross different regions. In contrast, the smaller window can exactly locate the objects edges, which can be seen from the target edge (see where the purple arrows points to). From the last column, we can see that compared to the other two parameter estimation methods, RWE can obtain accurate boundary with less isolated small regions (see the green rectangle). Note that the TLS cannot yield satisfying results without isolated small regions. The bottom three rows display the results of combining ITLS instead of TLS. We can see that the modified level set ITLS is robust to speckle noises (the segmentation results have no isolated small regions) even in a small window. In the context of the sliding window size is 3×3, although the combinatorial methods of MOM, ITLS and MLE, ITLS have good boundary location in the region where the purple arrows point to. However, these methods cannot acquire well segmentation results in green rectangles. In contrast, the combinatorial method of RWE, ITLS have an amazing result. In general, our proposed combinatorial method of RWE, ITLS achieves better segmentation performance and obtains much smoother contour than other two combinatorial methods.

To evaluate the accuracy performance, MSE was used for measuring the parameter estimation accuracy of Fig. 5.

TABLE 1. The MSE of estimated roughness parameter with different methods and different sliding window sizes.

methods	window sizes			
	9×9	7×7	5×5	3×3
MOM	1.1370	1.4422	2.4699	5.8896
MLE	0.4989	0.5033	0.5129	0.7948
RWE	1.3320	0.6573	0.3902	0.3765

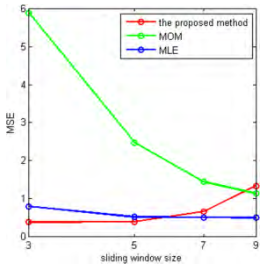

FIGURE 6. Overview of the MSE of estimated roughness parameter with different methods and different sliding window size.

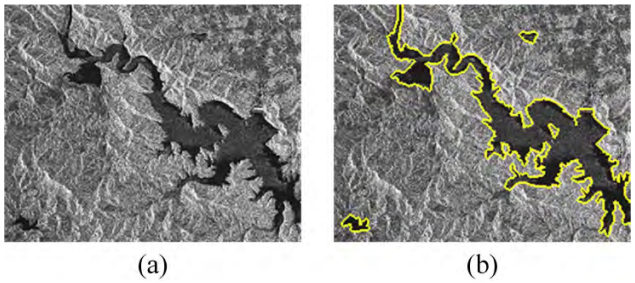

FIGURE 7. (a) is a real SAR image and (b) is its ground truth.

The smaller the value of MSE, the higher the accuracy of estimation. The results of MSE is described in Table 1. Fig. 6 shows the quantitative comparison.

Fig. 7(a) is a real SAR image: a 250×200 (pixels) image of Wuyang from a three-look HJ-1C S-band radar image with a spatial resolution of 5 m and Fig. 7(b) is its ground truth. Fig. 8 shows the segmentation results with different methods and sliding windows. The red, green, and purple regions are named as region A, B, and C respectively. The first three rows have the same segmentation method (TLS) and different estimation methods (MOM, MLE, and RWE). For the same rows, the segmentation results with large windows have less isolated small areas (region C), but lost many details of object edges (region A and B). Nevertheless, the segmentation results with small ones are just the opposite. This is because, for LTS, the larger the window is, the more noise it can suppress, but at the same time, the boundaries will be eroded. For the same column, the results with RWE have better segmentation with less isolated areas. The second three rows utilized ITLS. Obviously, for small windows, the method with ITLS and RWE not only obtain exact object edges, but also can remove isolate small regions.

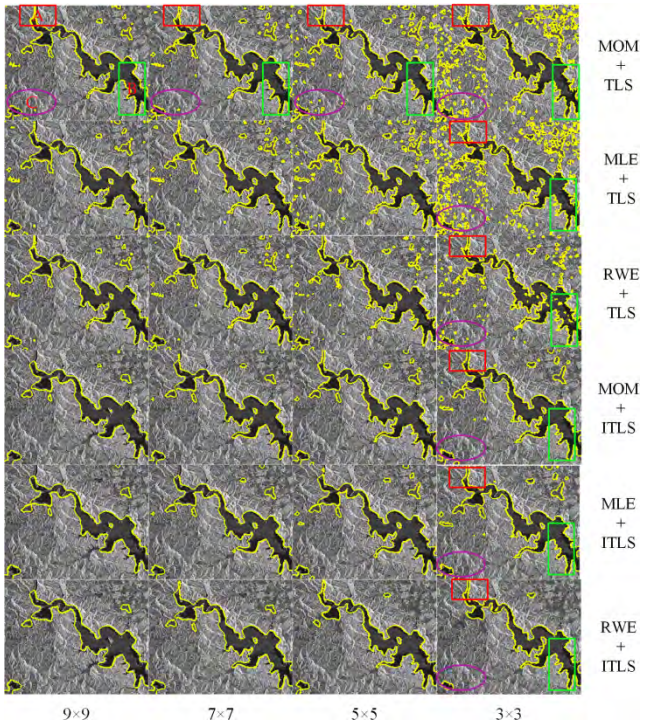

FIGURE 8. Segmentation results of Fig. 7(a) with different methods and different sliding windows. The sliding window size and the segmentation methods are at the bottom and right of the picture, respectively. The red, green and purple regions are named as region A, B, and C.

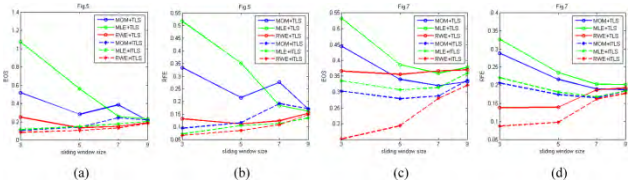

FIGURE 9. Overview of the EOS and RFE of Fig. 5 and Fig. 8: (a) the line chart of EOS of Fig. 5, (b) the line chart of RFE of Fig. 5, (c) the line chart of EOS of Fig. 8, (d) the line chart of RFE of Fig. 8.

To clearly demonstrate the segmentation performance about the above analysis and the results of synthetic and real SAR images, the EOS and RFE are used to measure the accuracy of segmentation results. Table 2 summarizes the EOS and RFE of Fig. 5 and Fig. 8. Fig. 9 can serve as a quantitative comparation. From Fig. 9, it is trivial to see that the EOS, RFE of the combinatorial method of RWE, ITLS are smaller than that of two other combinatorial methods.

From Table 2, we see that the proposed method achieves the best results with EOS = 0.0842, RFE = 0.0657 for simulated SAR image Fig. 4(a) and EOS = 0.1516, RFE = 0.0868 for real SAR image Fig. 7(a). We can conclude that our method can achieve outstanding segmentation results for both simulated and real SAR images.

C. COMPARATIVE EXPERIMENTS

1) SYNTHETIC SAR IMAGES

Fig. 10 exhibits the segmentation effect of our method on synthetic SAR images. Fig. 10(a1) is a low-contrast image

TABLE 2. The EOS and RFE of segmentation results both in Fig. 5 and Fig. 8 with different estimators and different sliding window size utilizing TLS and ITLS.

images	methods	window sizes							
		9×9		7×7		5×5		3×3	
		EOS	RFE	EOS	RFE	EOS	RFE	EOS	RFE
Fig 5	MOM+TLS	0.2131	0.1697	0.3868	0.2758	0.2835	0.2151	0.5186	0.3338
	MLE+TLS	0.2303	0.1618	0.2576	0.1846	0.5611	0.3512	1.0743	0.5163
	RWE+TLS	**0.1913**	**0.1539**	**0.1498**	**0.1234**	**0.1337**	**0.1111**	**0.2518**	**0.1313**
	MOM+ITLS	0.2169	0.1715	0.2447	0.1919	0.1419	0.1161	0.1050	0.0946
	MLE+ITLS	0.2033	0.1345	0.1759	0.1133	0.1483	0.1046	0.1158	0.0713
	RWE+ITLS	**0.1841**	**0.1482**	**0.1318**	**0.1080**	**0.1040**	**0.0855**	**0.0842**	**0.0657**
Fig 8	MOM+TLS	0.3327	0.1878	0.3195	0.1897	0.3400	0.2162	0.4442	0.2885
	MLE+TLS	0.3777	0.2018	0.3597	0.2025	0.3862	0.2348	0.5324	0.3268
	RWE+TLS	**0.3698**	**0.1925**	**0.3667**	**0.1875**	**0.3558**	**0.1392**	**0.3662**	**0.1376**
	MOM+ITLS	0.3367	0.1843	0.2875	0.1649	0.2787	0.1744	0.3030	0.2059
	MLE+ITLS	0.3591	0.1837	0.3142	0.1681	0.3065	0.1809	0.3356	0.2205
	RWE+ITLS	**0.3211**	**0.1774**	**0.2800**	**0.1615**	**0.1934**	**0.0974**	**0.1516**	**0.0868**

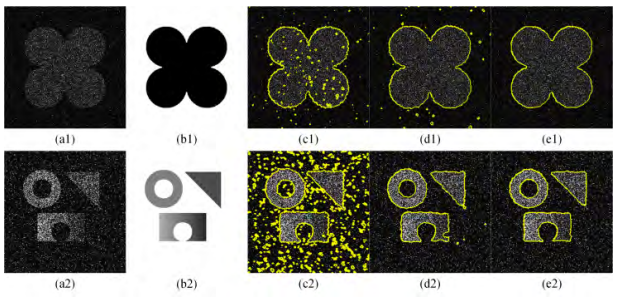

FIGURE 10. (a) the original image, (b) the ground truth, (c) and (d) the segmentation results by [17] and [9], (e) the result with RWE and the proposed level set method (ITLS).

TABLE 3. Results of EOS and RFE from different methods tested on Fig. 10.

SAR images	[17]		[9]		the proposed	
	EOS	RFE	EOS	RFE	EOS	RFE
Fig.10(a1)	0.0342	0.0160	0.0287	0.0247	0.0171	0.0107
Fig.10(a2)	0.2835	0.2151	0.1590	0.0693	0.0842	0.0657

and Fig. 10(a2) is an image with weak edge. In these images, different objects possess distinct parameters, where $L = 1$, $\alpha \in (-1.5, -3, -4.5, -6)$ and $\gamma \in (1, 5, 10)$. Fig. 10(c)-(e) are the segmentation results by [17] and [9] and the proposed method in this paper. We can see that the method proposed in this paper is more robust to speckle noise than the segmentation method in [17] from these experimental results. Beyond that, our method realized more smooth segmentation than the method in [9]. Table 3 displays the data comparison of the segmentation results. In Table 3, EOS and RFE are utilized to evaluate the performance on synthetic images.17 EOS and RFE are calculated by formulas (22) and (23) respectively. Obviously, the EOS and RFE of our method are 0.0171 and 0.0107 for Fig. 10(a1) and 0.0842 and 0.0657 for Fig. 10(a2) and they are the smallest of the three methods. Altogether, we can acquire the conclusion that our method has nice segmentation results on simulated images with low contrast and weak edge.

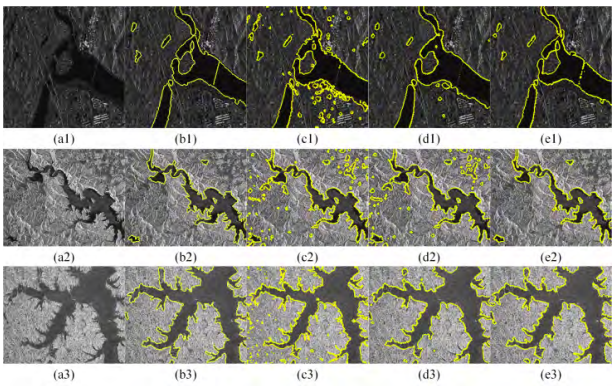

FIGURE 11. (left to right) (a1) - (a3) the original image, (b1) - (b3) the ground truth, (c1) - (c3) and (d1) - (d3) the segmentation results by [17] and [9], (e1)- (e3) the result with RWE and ITLS (our method).

2) REAL SAR IMAGES

In this section, the proposed method was applied to real mutilook intensity SAR images. Comparisons among the proposed method, the methods in [9] and [17] are shown in Fig. 11. There are three real SAR images in Fig. 11(a1)-(c1): an image of Miyun station (256×256) from a three-look HJ-1C S-band radar image, with a spatial resolution of 5 m, an image of Wuyang (250×200) from a three-look HJ-1C S-band radar image with a spatial resolution of 5 m, an image of Liangzi Lake (250×200) from a three-look HJ-1C S-band radar image with a spatial resolution of 5 m. The second column is the segmentation ground truth provided by an SAR image interpretation expert.

TABLE 4. Values of RFE from different methods tested on Fig. 11.

SAR images	RFE		
	[17]	[9]	the proposed
Fig.11(a1)	0.1622	0.1339	0.0758
Fig.11(a2)	0.2162	0.2706	0.0653
Fig.11(a3)	0.0901	0.0895	0.0483

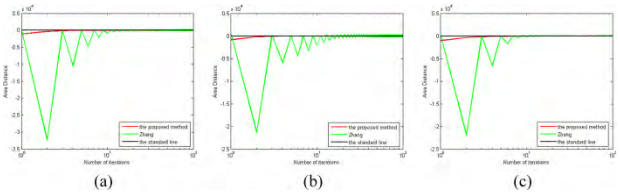

FIGURE 12. Overview of area distance changing. (a), (b) and (c) are the charts of Fig. 11(a1), (a2) and (a3) respectively.

The third column and fourth column display the comparison method in [17] and [9]. The final column shows the experimental results by the proposed method. In Fig. 11, we can see that (c1) (c2) and (c3) exist lots of isolated small areas, which verified that MOM is not suitable to estimate the parameters of $\mathcal{G}_I^0$ distribution used for SAR images. Table 4 displays the values of RFE from different methods tested on Fig. 11. From Fig. 11 and Table 4, we can conclude that our method can achieve more accurate segmentation results with lower RFE.

D. STABILITY ANALYSIS

Stability is an extremely important evaluation performance for the level set to segment SAR images. Stable segmentation results mean that the method is robust to speckle noise. However, many papers ignore the assessment of the performance of the level set. In this section, we will discuss the stability of our method.

Firstly, for the comparison of stability, we proposed the area distance (D_A) to evaluated the stability performance of level sets. The D_A is computed by

$$D_a(i) = \begin{cases} A_{i+1} - A_i, & i < I_{\max} \\ D_a(I_{\max} - 2), & i = I_{\max} \end{cases} \tag{24}$$

where $D_a(i)$ is the i-th D_a value, $I_{\max}$ is the maximum number of iterations, A_i is the area of the segmented region of the i-th division. We compared the stability of the level set proposed in [9] and ITLS. In Fig. 12, (a), (b) and (c) are the charts of area distance of level set evolution in [9] and ITLS corresponding to Fig. 11(a1), (a2) and (a3). $I_{\max}$ is set as 100. Fig. 12 presents the change in the area of the partitioned region between each iteration of the evolution. Evidently, at the end of the evolution of the contour, the area of the segmented region of our method tends to be stable, and the method of [9] appears a lot of fluctuations. This also shows that our method can achieve a more stable segmentation result. Furthermore, our method can achieve more stable splitting results compared to the method in [9].

V. CONCLUSIONS

In this paper, we introduced a precise and stable segmentation methodology based on the Random Weighting Estimator, entropy processing of SAR data modeled by $\mathcal{G}_I^0$ distribution and the improved threshold-based level set segmentation method. On synthetic SAR images, for small sliding window size, we verified that RWE has a higher estimated accuracy compared to MOM and MLE. The improved threshold-based level set segmentation method achieved more stable SAR image segmentation. The segmentation results on both simulated and real SAR images confirm that our segmentation methodology outperforms others.

ACKNOWLEDGMENT

The authors gratefully acknowledge Cuihuan Wang for the experimental assistance. In addition, the authors are also grateful to the reviewers for their valuable comments, which greatly improved the quality of this paper.

REFERENCES

[1] C. Oliver, S. Quegan, *Understanding Synthetic Aperture Radar Images*. Rijeka, Croatia: SciTech, 2004.
[2] R. Fjortoft, A. Lopes, J. Bruniquel, and P. Marthon, "Optimal edge detection and edge localization in complex SAR images with correlated speckle," *IEEE Trans. Geosci. Remote Sens.*, vol. 37, no. 5, pp. 2272–2281, Sep. 1999.
[3] M. T. Alonso, C. López-Martínez, J. J. Mallorquí, and P. Salembier, "Edge enhancement algorithm based on the wavelet transform for automatic edge detection in SAR images," *IEEE Trans. Geosci. Remote Sens.*, vol. 49, no. 1, pp. 222–235, Jan. 2011.
[4] M. Modava and G. Akbarizadeh, "Coastline extraction from SAR images using spatial fuzzy clustering and the active contour method," *Int. J. Remote Sens.*, vol. 38, no. 2, pp. 355–370, Dec. 2016.
[5] J. Gu, L. Jiao, S. Yang, F. Liu, B. Hou, and Z. Zhao, "A multi-kernel joint sparse graph for SAR image segmentation," *IEEE J. Sel. Topics Appl. Earth Observ. Remote Sens.*, vol. 9, no. 3, pp. 1265–1285, Mar. 2016.
[6] Y. Li, J. Li, and M. A. Chapman, "Segmentation of SAR intensity imagery with a Voronoi tessellation, Bayesian inference, and reversible jump MCMC algorithm," *IEEE Trans. Geosci. Remote Sens.*, vol. 48, no. 4, pp. 1872–1881, Apr. 2010.
[7] S. Luo, L. Tong, and Y. Chen, "A multi-region segmentation method for SAR images based on the multi-texture model with level sets," *IEEE Trans. Image Process.*, vol. 27, no. 5, pp. 2560–2574, May 2018.
[8] J. Liu, X. Wen, Q. Meng, H. Xu, and L. Yuan, "Synthetic aperture radar image segmentation with reaction diffusion level set evolution equation in an active contour model," *Remote Sens.*, vol. 10, no. 6, p. 906, Jun. 2018.
[9] X. Zhang, X. Wen, H. Xu, and Q. Meng, "Synthetic aperture radar image segmentation based on edge-region active contour model," *J. Appl. Remote Sens.*, vol. 10, no. 3, p. 036014, Aug. 2016.
[10] B. Wang and G. Wang, "A G$^{\Gamma}$D based level set method for target segmentation in high resolution SAR images," in *Proc. 2nd Int. Conf. Frontiers Sensors Technol. (ICFST)*, Apr. 2017, pp. 256–259.
[11] I. R. Joughin, D. B. Percival, and D. P. Winebrenner, "Maximum likelihood estimation of K distribution parameters for SAR data," *IEEE Trans. Geosci. Remote Sens.*, vol. 31, no. 5, pp. 989–999, Sep. 1993.
[12] H. C. Li, W. Hong, Y. R. Wu, and P. Z. Fan, "On the empirical-statistical modeling of SAR images with generalized gamma distribution," *IEEE J. Sel. Topics Signal Process.*, vol. 5, no. 3, pp. 386–397, Jun. 2011.
[13] T. Bucciarelli, P. Lombardo, C. J. Oliver, and M. Perrotta, "A compound Weibull model for SAR texture analysis," in *Proc. IEEE Int. Geosci., Remote Sens. Symp.*, Jul. 1995, pp. 181–183.
[14] A. C. Frery, C. da Costa F. Yanasse, and S. J. S. Sant'Anna, "Alternative distributions for the multiplicative model in SAR images," in *Proc. Int. Geosci. Remote Sens. Symp. Quant. Remote Sens. Sci. Appl. (IGARSS)*, Jul. 1995, pp. 169–171.
[15] A. C. Frery, H.-J. Muller, C. C. F. Yanasse, and S. J. S. Sant'Anna, "A model for extremely heterogeneous clutter," *IEEE Trans. Geosci. Remote Sens.*, vol. 35, no. 3, pp. 648–659, May 1997.

[16] R. C. P. Marques, F. N. Medeiros, and J. S. Nobre, "SAR image segmentation based on level set approach and $\mathcal{G}A^0$ model," *IEEE Trans. Pattern Anal. Mach. Intell.*, vol. 34, no. 10, pp. 2046–2057, Oct. 2012.
[17] R. H. Nobre, F. A. A. Rodrigues, R. C. P. Marques, J. S. Nobre, J. F. S. R. Neto, and F. N. S. Medeiros, "SAR image segmentation with Rényi's entropy," *IEEE Signal Process. Lett.*, vol. 23, no. 11, pp. 1551–1555, Nov. 2016.
[18] F. A. A. Rodrigues, J. F. S. R. Neto, R. C. P. Marques, F. N. S. de Medeiros, and J. S. Nobre, "SAR image segmentation using the roughness information," *IEEE Geosci. Remote Sens. Lett.*, vol. 13, no. 2, pp. 132–136, Feb. 2016.
[19] C.-H. Wang, X.-B. Wen, and H.-X. Xu, "A robust estimator of parameters for $\mathcal{G}$I0-modeled SAR imagery based on random weighting method," *EURASIP J. Adv. Signal Process.*, vol. 2017, no. 1, p. 22, Feb. 2017.
[20] Z. G. Zheng, "Random weighting method," (in Chinese), *ACTA Mathematicae Applicatae Sinica*, vol. 10, no. 2, pp. 247–253, 1987.
[21] Z. G. Zheng and D. S. Tu, "Random weighting method in regression models," *Sci. China, Ser. A*, vol. 31, no. 12, pp. 1442–1459, 1988.
[22] J. Feng, Z. Cao, and Y. Pi, "A G0 statistical model based level set approach for SAR image segmentation," in *Proc. Eur. Conf. Synth. Aperture Radar*, Jun. 2010, pp. 1–4.
[23] M. E. Mejail, J. C. Jacobo-Berlles, A. C. Frery, and O. H. Bustos, "Classification of SAR images using a general and tractable multiplicative model," *Int. J. Remote Sens.*, vol. 24, no. 18, pp. 3565–3582, Jan. 2003.
[24] M. Mejail, J. Gambini, N. Goussies, M. E. Buemi, and J. C. Jacobo, "SAR image segmentation using a fast level set technique," in *Proc. Eur. Conf. Synth. Aperture Radar (VDE)*, 2008, pp. 1–4.
[25] H. Zou, X. Qin, H. Kang, S. Zhou, and K. Ji, "A PDF-based SLIC superpixel algorithm for SAR images," in *Proc. IEEE Int. Geosci. Remote Sens. Symp. (IGARSS)*, Jul. 2016, pp. 6823–6826.
[26] J. A. Sethian, *Level Set Methods and Fast Marching Methods: Evolving Interfaces in Computational Geometry, Fluid Mechanics, Computer Vision, and Materials Science*. Cambridge, U.K.: Cambridge Univ. Press,1998.
[27] B. Huang, H. Li, and X. Huang, "A level set method for oil slick segmentation in SAR images," *Int. J. Remote Sens.*, vol. 26, no. 6, pp. 1145–1156, Mar. 2005.
[28] C. Li, C.-Y. Kao, J. C. Gore, and Z. Ding, "Minimization of region-scalable fitting energy for image segmentation," *IEEE Trans. Image Process.*, vol. 17, no. 10, pp. 1940–1949, Oct. 2008.

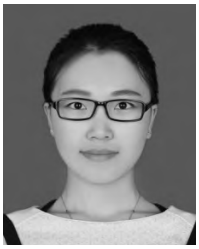

SHANSHAN LIN received the B.S. degree in computer science and technology from Qiqihar University, in 2016. She is currently pursuing the master's degree with the School of Computer Science and Engineering, Tianjin University of Technology. Her research interests include the segmentation and the classification of remote sensing images.

XIANBIN WEN received the Ph.D. degree from Northwestern Polytechnical University, Xi'an, China, in 2005. He is currently a Professor with the School of Computer Science and Engineering, Tianjin University of Technology, Tianjin, China. His research interests include image interpretation, machine learning, and information hiding.

HAIXIA XU received the M.Sc. degree in applied mathematics and the Ph.D. degree in computer science and technology from Northwestern Polytechnical University, China, in 2006 and 2009, respectively. She is currently an Associate Professor with the School of Computer Science and Engineering, Tianjin University of Technology, China. Her main research interests include image analysis, signal processing, and pattern recognition.

LIMING YUAN received the Ph.D. degree in computer science and technology from the Harbin Institute of Technology, China, in 2014. He is currently a Lecturer with the School of Computer Science and Engineering, Tianjin University of Technology, China. His research interests mainly include machine learning and image processing.

QINGXIA MENG received the M.S. degree in computer and communication engineering from the Tianjin University of Technology, Tianjin, China, in 2013, where she is currently pursuing the Ph.D. degree in computer science and technology. Her research interests include machine learning, image processing, remote sensing images, and synthetic aperture radars.